

Geophysical Research Letters®



RESEARCH LETTER

10.1029/2023GL107927

Key Points:

- Climate simulations reveal year-round cooling in the Northern Hemisphere high latitudes during the last glacial inception
- A refined angular calendar provides a tool to analyze the seasonal dynamics
- We identify the crucial role of the albedo feedback on the high-latitude radiative budget

Correspondence to:

S. Xu,
shan.xu@awi.de

Citation:

Xu, S., Krebs-Kanzow, U., & Lohmann, G. (2024). A seasonally delayed sea ice response and Arctic amplification during the last glacial inception. *Geophysical Research Letters*, *51*, e2023GL107927. <https://doi.org/10.1029/2023GL107927>

Received 22 DEC 2023

Accepted 16 MAY 2024

A Seasonally Delayed Sea Ice Response and Arctic Amplification During the Last Glacial Inception

Shan Xu¹ , Uta Krebs-Kanzow¹ , and Gerrit Lohmann^{1,2} 

¹Alfred Wegener Institute, Helmholtz Centre for Polar and Marine Research, Bremerhaven, Germany, ²University of Bremen, Bremen, Germany

Abstract The last glacial inception (LGI) marks the transition from the interglacial warm climate to the glacial period with extensive Northern Hemisphere ice sheets and colder climate. This transition is initiated by decreasing boreal summer insolation but requires positive feedbacks to stimulate the appearance of perennial snow. We perform simulations of LGI with climate model AWI-ESM-2.1, forced by the astronomical and greenhouse gas forcing of 115,000 years before present. To compare with the preindustrial (PI) simulation, we use a consistent definition of the seasons during the LGI and the PI and evaluate model output on an angular astronomical calendar. Our study reveals a prominent role of the sea-ice albedo feedback to amplify the delayed climate signal at polar latitudes. Through a radiative budget analysis, we examine that the ice-albedo feedback exceeds the shortwave radiative forcing, contributing to the cooling and high latitude snow built-up during LGI.

Plain Language Summary The onset of the last ice age marks the transition from the interglacial warm climate to the ice age with extensive Northern Hemisphere (NH) ice sheets and colder climate. This transition is initiated by decreasing boreal summer irradiance and reinforced by positive feedbacks. We perform climate simulations under the astronomical and greenhouse gas forcing, and use a consistent definition of seasons. Our study shows that a delayed ice-albedo feedback plays an important role in generating a cold NH climate.

1. Introduction

At the end of the last interglacial, the Earth gradually transitioned to a colder climate, the last glacial inception (LGI). Between 120 and 115 thousand years before present (ka), snow and ice sheets started to develop in Northern Hemisphere (NH), with ice nuclei first appearing over the Canadian Arctic islands, Labrador, northern continental Canada, continental western Siberia and Eurasian Arctic islands (Andrews & Barry, 1978; Clark et al., 1993; Lambeck et al., 2006; Mangerud & Svendsen, 1992; Svendsen et al., 2004). Different from most glacial periods, the LGI is characterized by its abruptness. By 110 ka, the ice sheets have expanded to cover approximately 70% of the area of Last Glacial Maximum (Stokes et al., 2012). Meanwhile, permanent sea ice thickened over the central Arctic and seasonal sea ice existed in the western Fram Strait (Stein et al., 2017). Marine sediments from the North Atlantic Ocean indicate that at the onset of the LGI the sea surface temperature was reduced at high latitudes (a cooling of around 5 K from present-day Balbon, 2000; Capron et al., 2014; Manthé, 1998). The northern high latitudes, exhibiting a stronger and earlier cooling signal, are key regions in this glaciation process.

Milankovitch (1941) postulated that the key drivers for glacial inceptions are the reduction in NH summertime insolation and the subsequent perennial snow accumulation. Previous model simulations with corresponding insolation forcing have shown a consistent cooling of temperature, an increase of snow cover and sea ice (e.g., Bahadory et al., 2021; Born et al., 2010), as also seen from proxies (Cortijo et al., 1999; Kremer et al., 2018; Stein et al., 2017). However, accurately capturing the specific location, range, and expansion rate of ice sheets is challenging due to model limitations and constraints of proxy data (e.g., Bahadory et al., 2021; Calov et al., 2005; Kageyama et al., 2004). This limits our understanding of glacial dynamics during the time period. Consequently, a key question is what positive feedback amplifies insolation forcing during the LGI. Furthermore, it remains unclear why the high-latitude cooling is prior to other regions. In addition to insolation, other contributions have been proposed, including albedo feedbacks (Calov et al., 2005; Kageyama et al., 2004), meridional temperature gradients (Young & Bradley, 1984), North Atlantic Ocean circulation (Imbrie et al., 1992), atmospheric circulation (Lohmann, 2017), sea ice feedback (Lachniet et al., 2017; Vavrus, 1999; Yoshimori et al., 2002), vegetation

© 2024. The Authors. Geophysical Research Letters published by Wiley Periodicals LLC on behalf of American Geophysical Union.

This is an open access article under the terms of the [Creative Commons Attribution License](https://creativecommons.org/licenses/by/4.0/), which permits use, distribution and reproduction in any medium, provided the original work is properly cited.

changes (De Noble et al., 1996; Gallimore & Kutzbach, 1996; Kageyama et al., 2004; Meissner et al., 2003; Yoshimori et al., 2002) etc.

Furthermore, most climate simulation studies analyze their model output based on the classical “fixed-days” calendar, which cannot represent the seasonal dynamics in paleo times (e.g., Joussaume & Braconnot, 1997; Kutzbach & Gallimore, 1988; Shi, Werner, Wang, et al., 2022). This approach might even lead to misinterpretations in climate patterns, such as temperature amplification, bipolar seesaw and global monsoon (Bartlein & Shafer, 2019). This bias is especially pronounced in periods like LGI. The orbital forcing during the LGI entails weak boreal summer insolation at high latitudes on NH hemisphere due to a lower-than-present obliquity and a higher-than-present eccentricity, additionally increased Earth's distance from the Sun in boreal summer (like today's boreal summer occurs near aphelion). The high eccentricity causes the orbital speed of the Earth around the Sun to be reduced in boreal summer and increased in boreal winter, which, with respect to today's calendar, implies a shift of the solstices and the related seasons. Therefore, misleading biases occur if we apply today's classical calendar to the seasonal cycle study of LGI.

In this paper, we conduct model simulations of preindustrial (PI) and LGI with a coupled earth system model. By focusing on the NH high-latitude feedbacks and employing a refined astronomical calendar, we aim to bridge the gap in understanding the seasonal dynamics of paleo times, particularly during the LGI.

2. Methods and Experiments

2.1. Model and Experiment Design

The model employed in this study is the state-of-the-art coupled Earth System Model AWI-ESM-2.1 (Sidorenko et al., 2019). AWI-ESM-2.1 is an atmosphere-ocean-land-sea ice model, which consists of the Finite Element Sea ice-Ocean Model FESOM-2.0 (Danilov et al., 2017) and ECHAM-6.3 for the atmosphere, vegetation and land surface (Stevens et al., 2013). The coupling between FESOM and ECHAM is achieved via the parallel OASIS3-MCT coupler (Valcke, 2013). The timestep of ECHAM is 450 s and the FESOM timestep is 30 min, and the ocean and atmosphere are coupled every 6 hr via the OASIS3-MCT coupler. ECHAM was run at T63 spectral resolution with 47 vertical levels. The ocean model FESOM uses an unstructured mesh CORE-II, with resolution varying from nominal one degree in the interior of the ocean to 1/3° in the equatorial belt and 24 km north of 50°N (Sidorenko et al., 2019). This model has been evaluated in terms of its mean state and long-term drift under PI forcing and is proved to have good capability of modeling the main characteristics in the atmosphere and ocean (Sidorenko et al., 2019). AWI-ESM has also been successfully applied for different paleoclimate periods (Shi et al., 2020; Shi & Lohmann, 2016; Shi, Werner, Wang, et al., 2022; Shi, Werner, Krug, et al., 2022).

To understand the feedbacks during the LGI, we conduct two simulations based on the modern topography with orbital (Berger, 1978) and astronomical forcing (Köhler et al., 2017) fixed at pre-industrial (ClimPI, eccentricity = 0.01672, obliquity = 23.45, precession = 282.04, CO₂ = 284 ppm, CH₄ = 808 ppb, N₂O = 273 ppb) and 115 ka (Clim115, eccentricity = 0.04142, obliquity = 22.41, precession = 291.01, CO₂ = 274 ppm, CH₄ = 498 ppb, N₂O = 252 ppb). Both simulations run for 1,200 model years. Daily outputs are provided for implementation of the calendar methods. The analysis presented in this study are based on the average mean of the last 50 years data from each simulation.

2.2. Calendar Effect

As discussed, applying today's fixed-day calendar to paleoclimate could result in significant bias, commonly expressed as “paleo calendar effect” (Bartlein & Shafer, 2019). To address this issue, our study adopts the “fixed-angular” calendar (hereafter angular calendar), aligned more closely with the orbital variations of Earth. Angular calendar replaces the traditional fixed-day definition with angular measurements based on Earth's orbit. Each year is divided into 360°, consequently 1° corresponding to one day, each 30° to one month, and 90° to one season. This provides a more accurate representation of the actual length of months and seasons in paleo times. In contrast to the classical calendar where boreal vernal equinox is fixed at March 21st, We align the angle of equinox with the angle of today's calendar. Different from the calendar adjustment methods by Pollard & Reusch, 2002, Timm et al., 2008; Chen et al., 2011, we also apply this approach for present-day climate.

We use daily model output to redefine the months of the year based on the angular calendar for both ClimPI and Clim115 experiments. In the PI scenario, the redefined month lengths from January to December are 29, 30, 30,

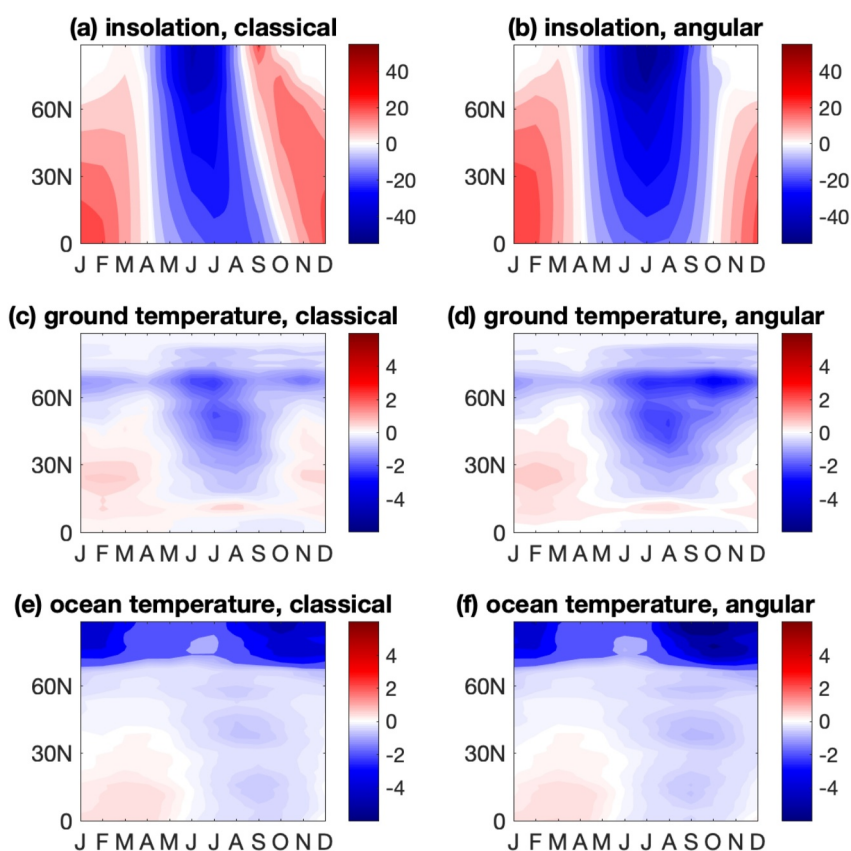


Figure 1. Annual cycle of zonal-mean changes between LGI and PI: panel (a–b), for incoming solar radiation at the top of the atmosphere (W/m^2); panel (c–d), for 2 m temperature over land (K); panel (e–f), for 2 m temperature over ocean and sea ice-covered areas (K). Left panels use classical fixed-day calendar. Right panels use the angular calendar.

31, 31, 31, 31, 31, 31, 30, 30, and 30 days, respectively. For the 115 ka scenario, the new month lengths are 28, 28, 29, 31, 32, 33, 33, 33, 31, 30, 29, and 28 days. A respective redefinition of seasons results in a 6-day-longer summer and 5-day-shorter winter season in the LGI scenario relative to PI.

Figures 1a and 1b shows the annual cycle of zonal-mean changes of insolation between LGI and PI. The incoming solar radiation at the top of the atmosphere in LGI compared with PI is primarily characterized by a decreased boreal summer insolation and an enhanced winter insolation, resulting in a weak seasonal contrast on NH hemisphere. The calendar adjustment reveals more symmetric seasonal contrasts and latitudinal distribution of insolation, such as the elimination of dipole pattern in autumn (Figure 1), enhancing a more direct comparison between the two climates. The angular calendar affects the seasonal means of surface temperature of both periods (Figure 2) but is more pronounced for LGI. It is most clearly visible over land in summer and autumn (Figure 2), where significant temperature differences can be observed. Additionally, it is crucial to mention that our choice of the boreal vernal equinox as the reference point impacts the distribution of paleo calendar effect, with the most prominent seasonal discrepancies observed during autumn. Only model results based on the angular calendar are presented below.

3. Results

3.1. Decoupling Between Insolation and Temperature in the Arctic Winter

As seen from Figure 3, the temperatures over land and ocean have a distinct response to insolation. Thus, we compare the near surface (2 m) temperature over land and ocean separately. The land temperature changes mainly follow the seasonal cycle of insolation anomalies in the low and middle latitudes with a lag of 1 month (Figure 1). The minimum 2 m temperature anomaly over land is seen in August with an average 0.5 K cooling, while the maximum anomaly is in February with a 0.1 K warming. However, at high latitudes, the temperature anomaly

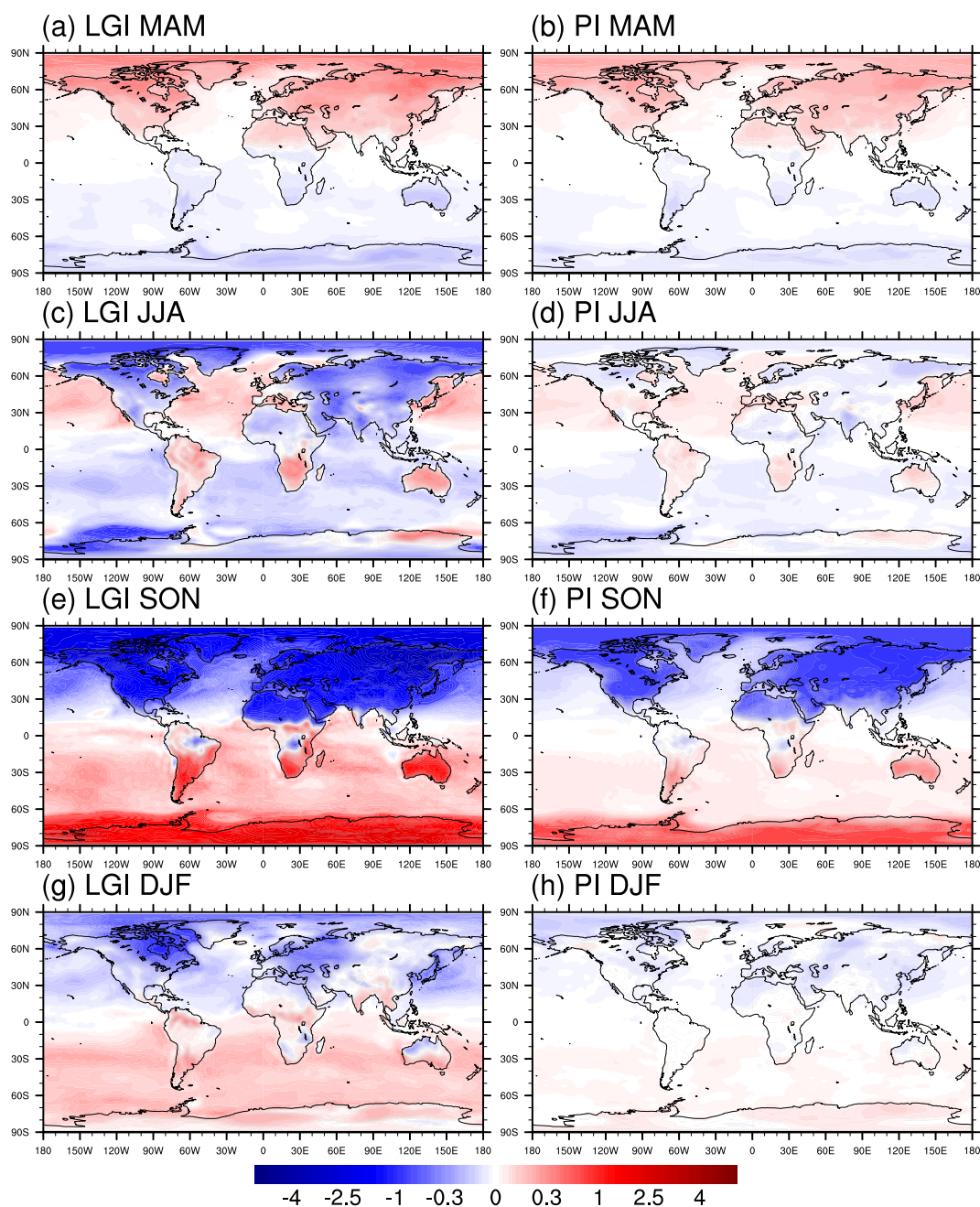


Figure 2. Paleo calendar effect on 2 m temperature in K during LGI (left panel) and PI (right) in different seasons. Paleo calendar effect is defined by the anomaly between angular calendar and classical calendar.

does not follow the seasonality of the insolation anomaly, and there is an anomalous cooling over the whole year. The zonal mean temperature north of the polar circle is about 2 K colder from November to March relative to the PI, despite a slight increase of insolation in the same months across all latitudes of the NH. The minimum temperature over the Arctic realm is seen in October, delayed by 2 months after minimum insolation change.

SST anomalies at low latitudes and parts of mid-latitudes south of 45°N reflect the LGI insolation anomaly with warmer winters and cooler summers, but exhibit a pronounced 2–3 months seasonal lag. North of 45°N, an anomalous cooling is observed over the whole year, and the minimum temperature lags the minimum insolation by 2–4 months. North of 67°N, a remarkable Arctic cooling exceeds the decrease of temperature at mid-latitudes

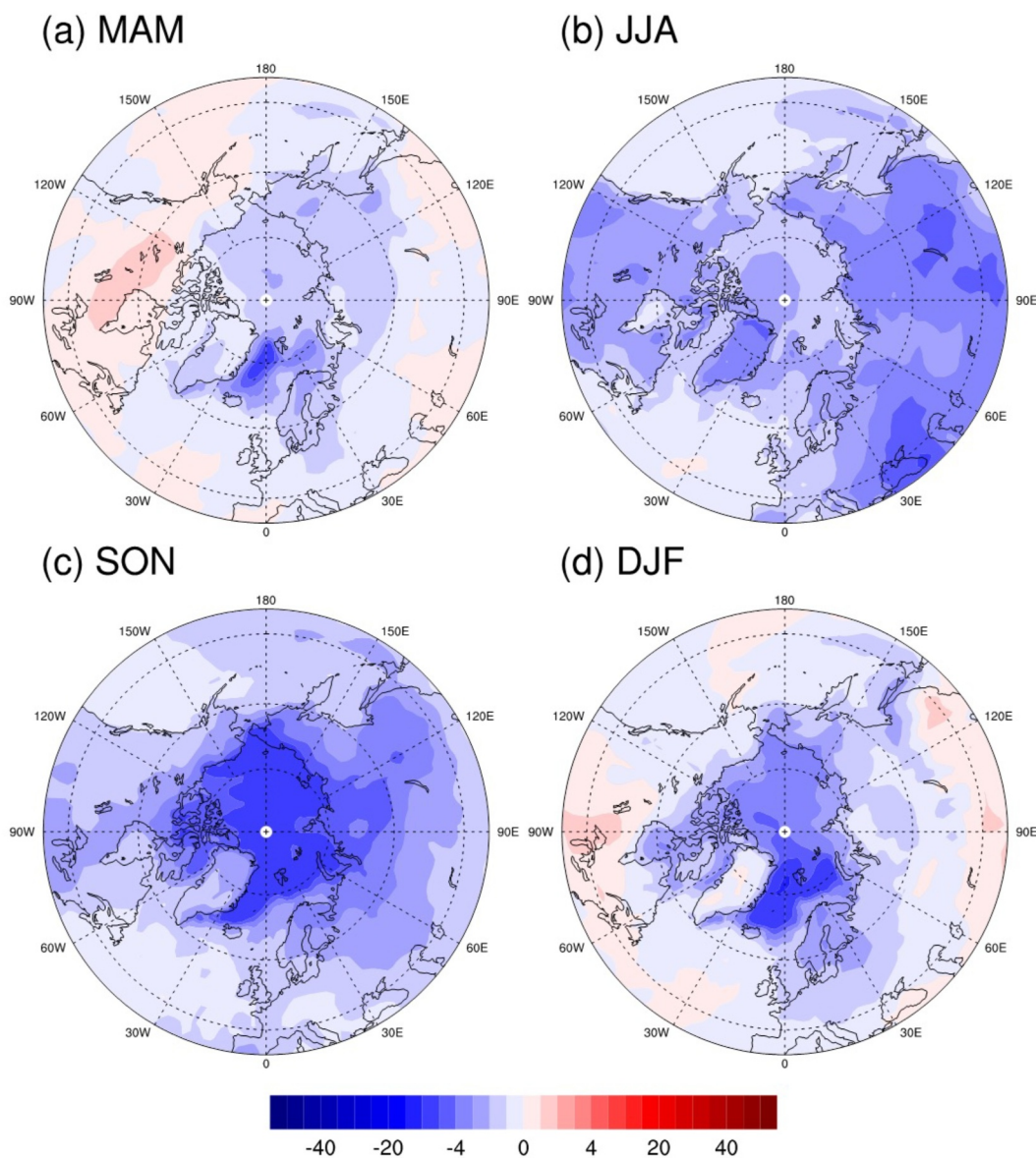


Figure 3. Near-surface 2 m temperature (K) differences between LGI and PI for different seasons. Seasons are defined by the angular calendar.

by about 3 K in winter (October to March). This cooling closely traces sea ice edges (Figure 4), which indicates that sea ice might play an important role on the decoupling between insolation and temperature during LGI.

3.2. The Albedo Response

The strong reduction in boreal summer insolation results in a weekend melt season and an expanded sea ice cover in the Arctic in Clm115. The contour of 50% sea ice cover fraction extends toward the coasts in the Canadian Arctic and East Siberia Sea and shifts toward lower latitudes in the Bering Strait and Greenland and Barents Sea. In the following autumn and winter, the less pronounced melt season further facilitates the formation of sea ice. In October, the Arctic sea-ice area anomaly reaches its maximum, concurrently and spatially correlated with the lowest Arctic temperature anomalies. However, the Norwegian Sea and western Barents Sea remain mostly ice free throughout the year in both experiments, which might be associated with a vigorous North Atlantic Current (Born et al., 2010).

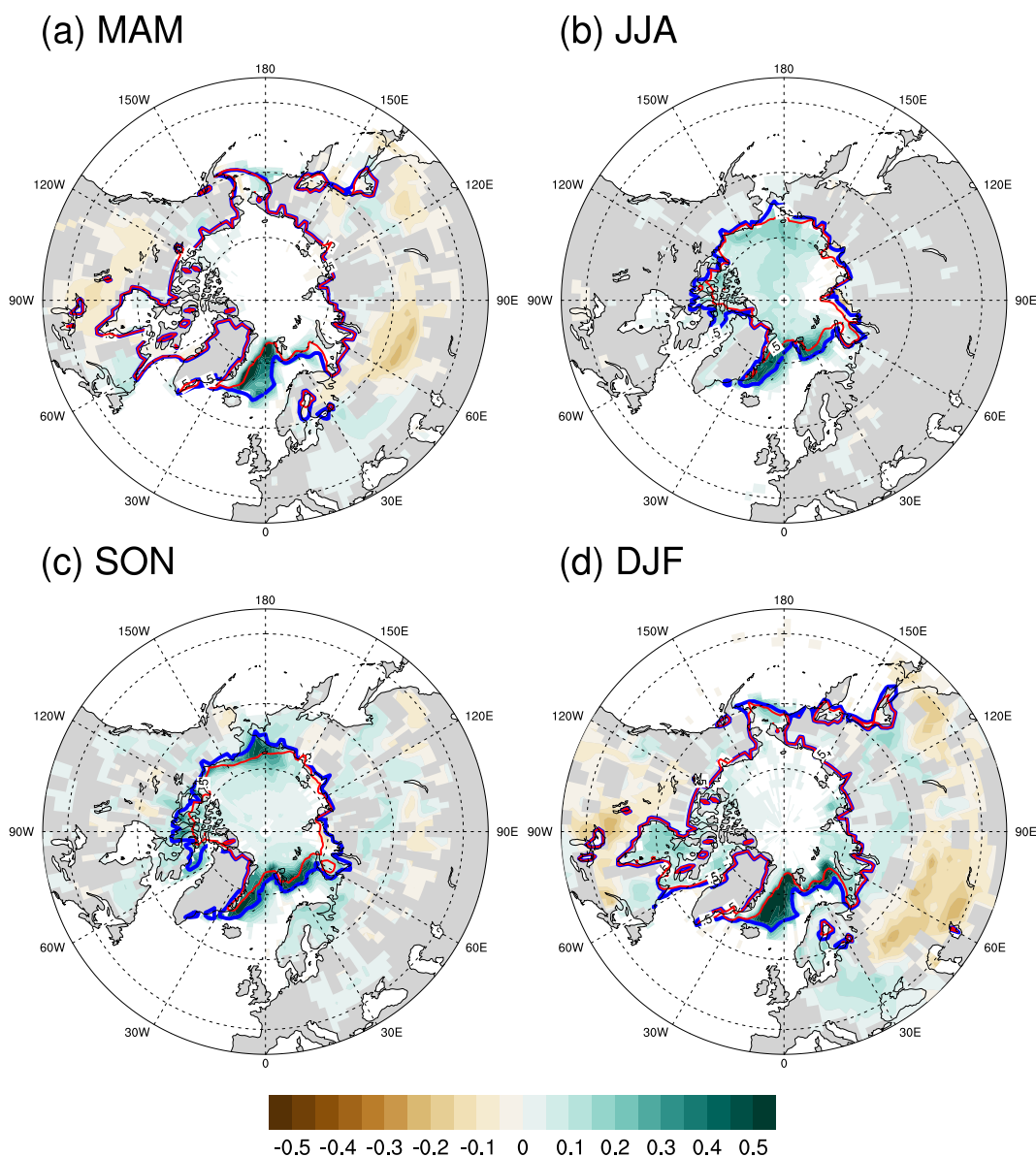


Figure 4. Albedo and sea ice changes between LGI and PI, also in the angular calendar. Shading indicates change in albedo, quantified as percentage. The thick blue and thin red curves indicate areas covered by more than 50% sea ice during LGI and PI, respectively.

In consequence albedo over the Arctic ocean (Figure 4) shows pronounced positive anomalies where sea-ice margins have advanced, for example, in the Greenland Sea. Albedo anomalies over land are weak and heterogeneous by comparison. Albedo is increased in autumn and winter and, to some extent, in spring over Nunavut, eastern Quebec, and small regions on Baffin Island, Scandinavia, and north-eastern Siberia. As precipitation is reduced over most parts of the Arctic land surfaces due to the colder climate, this is indicative of earlier snow cover or later onset of the melt season. The spatial albedo pattern is consistent with ice sheet reanalysis data which indicates formation of large ice caps and glaciers during this period in these regions (Batchelor et al., 2019). There is however no indication of extensive perennial snow cover in our Clm115 experiment as the simulated climate is too warm in summer and resolution is not sufficient to resolve high altitude mountain ranges.

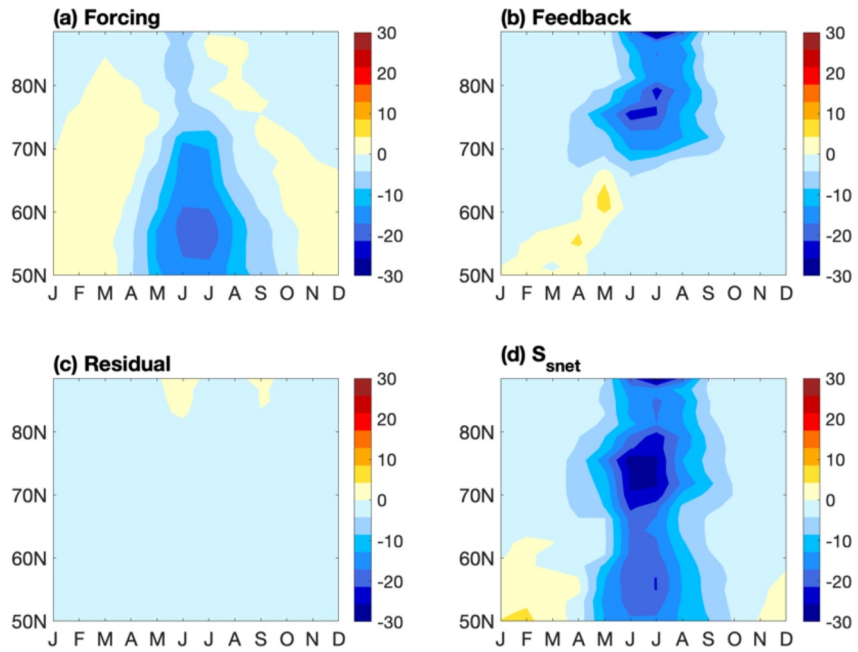


Figure 5. Results from the shortwave radiation budget analysis, panel (a–d) shows annual cycle of zonal mean surface radiative forcing, albedo feedback, residual effect, and the anomaly of net surface shortwave radiation, unit in W/m^2 .

3.3. Radiative Budget Analysis

In order to understand the relative contribution of radiative forcing on climate change, we analyze the energy budget of the Earth's surface from shortwave radiation by separating forcing and feedback components. For a given phase of the seasonal cycle, the surface shortwave radiation budget is

$$S_{snet} = S_{sd} * (1 - A) \quad (1)$$

where S_{snet} is the net surface shortwave radiation, S_{sd} is the surface downward shortwave radiation, and A is the surface albedo. These variables can also be represented as climatological mean from a common reference and their corresponding anomalies with respect to this reference. In this way, the LGI anomaly in S_{snet} can be expressed as

$$S'_{snet} = S'_{sd} * (1 - \bar{A}) - \bar{S}_{sd} * A' - S'_{sd} * A' \quad (2)$$

where the overbar indicates the climatological mean under PI and the primed quantities represent the anomalies between LGI and PI. The anomaly of S_{snet} is decomposed into three terms. The first term on the right hand side is the shortwave radiative forcing, which is the effect of the anomalous radiation. The second term stands for the radiative feedback resulting from albedo changes that modify the surface radiation budget. The third term on the right hand is the residual term, including nonlinear processes resulting from the combined effect of surface radiation anomalies and albedo anomalies. Here, we call the above three terms surface radiative forcing, albedo feedback, and residual effect in our later discussion.

Our radiation budget analysis follows Jackson and Broccoli (2003). The only difference is in distinguishing the mean and variation of quantities. In their work, they determined the overbar as a long-term mean and the primed quantities as the anomaly regarding the mean value. To have a direct comparison with the profile of incoming insolation and temperature, we integrate Equation 2 zonally over both land and ocean areas. Figure 5 shows the latitudinal profile of all the decomposition components on the right hand side of Equation 2. The surface shortwave radiative forcing decreases the most at $\sim 55^\circ N$ in summer, whereas changes in wintertime are relatively small. In higher latitudes, the albedo feedback overwhelms the weak radiative forcing due to the pronounced

difference in summer sea ice coverage: forcing only contributes less than -5 W/m^2 to the total budget, while the feedback amounts to up to -30 W/m^2 , resulting in a significant reduction of net surface radiation during May to September (MJJAS).

In contrast to higher latitudes on the NH, the albedo feedback is not a factor south of 67°N , where summer sea ice does not exist during both periods. The magnitude of the residual term is much smaller than the other two terms, indicating that the combined effect from both shortwave radiative forcing and albedo feedback has a negligible contribution to the total radiation budget.

4. Discussion

We apply the coupled climate model AWI-ESM to study the mechanisms of regional cooling during the LGI. The LGI simulation exhibits a weakened seasonal cycle in temperature with the Arctic being colder than PI throughout the year. Through a radiative budget analysis, we find that in high latitudes albedo feedback exceeds the shortwave radiative forcing, contributing to the cooling in high latitude regions during the LGI, which favors a “glaciation-friendly climate” at that time.

It is interesting to discuss the geological evidences of the high-latitude climate of the LGI. During the transition from the last interglacial to the inception, the sea-ice cover was indeed quite variable (Kremer et al., 2018; Stein et al., 2017). During the early mid part of the last interglacial, sediments show a reduction in sea ice which might have been even less extensive than today (Van Nieuwenhove et al., 2011; Irvali et al., 2016; Kremer et al., 2018; Stein et al., 2017). During the late part of last interglacial and the transition to LGI, a major ice sheet advance is observed in the western continental margin of Svalbard (Mangerud et al., 1996, 1998) and an extended sea-ice cover at the northern and western Barents Sea continental margin (Kremer et al., 2018; Stein et al., 2017). This agrees with our model simulations on LGI showing an extended sea-ice cover relative to PI. In addition, the response of snow in our simulations also shows favorable glaciation conditions. The changes on sea ice strongly influence the radiation budget through albedo feedback over the entire Arctic, and thereby have a significant impact on the temperature.

Previous model studies found that the distribution of sea ice under PI conditions and its sensitivity to different forcing is highly model dependent (Kageyama et al., 2020). In particular, unlike other models, AWI-ESM does not exhibit pronounced permanent sea ice in the Baffin and Hudson Bay, which could imply that the sensitivity of the high latitude North America is also model dependent, especially considering that more sea ice in the Baffin Bay might have an effect on the climate on the North America continent. Therefore, the spatial fingerprint of our result demonstrates that sea ice has a strong amplifying effect on the regional climate response.

Although albedo feedback is a key driver of Arctic cooling, the cloud feedback exhibits a counteracting effect, potentially mitigating the overall cooling effect (Erb et al., 2013; Jochum et al., 2012; Sagoo et al., 2021). This interaction between albedo and cloud feedback underscores the intricate dynamics of the Arctic climate, emphasizing albedo feedback as the primary mechanism behind Arctic cooling patterns, notwithstanding the tempering effects of cloud feedback. The cloud feedback is not a focus of our research.

5. Conclusions

We analyze our climate model AWI-ESM for LGI and PI conditions. Our main findings are:

1. The LGI shows a more “glaciation-friendly climate” compared to PI: a year-round NH anomalous cooling and a delayed temperature signal in response to insolation through sea ice.
2. The positive effect of albedo dominates the radiative budget on NH high latitudes, associated to expanded sea ice. This is consistent with proxy indicators.
3. A paleo-calendar based on fixed-angular is recommended for studying seasonal paleoclimate, especially if eccentricity and precession are different from present.

A logical next step is to investigate a coupled ice sheet-climate model (e.g., Ackermann et al., 2020) in a transient mode starting from the last interglacial to investigate the feedbacks identified here.

Data Availability Statement

Data for this research are available for download at Zenodo (Xu et al., 2024). Software for this research is available in Shi, Werner, Krug, et al. (2022).

Acknowledgments

We acknowledge the support from Alfred Wegener Institute Helmholtz Center for Polar and Marine Research in Bremerhaven Germany. We also would like to thank Anthony J. Broccoli and another anonymous reviewer for their constructive comments that improved this manuscript. Shan Xu is funded by the China Scholarship Council. Uta Krebs-Kanzow and Gerrit Lohmann acknowledge the Helmholtz Climate Initiative REKLIM (Regional Climate Change), Bundesministerium für Bildung und Forschung (PalMod project) and the PoF IV “Changing Earth—Sustaining our Future” research program of the Alfred Wegener Institute. Open Access funding enabled and organized by Projekt DEAL.

References

- Ackermann, L., Danek, C., Gierz, P., & Lohmann, G. (2020). AMOC Recovery in a multicentennial scenario using a coupled atmosphere-ocean-ice sheet model. *Geophysical Research Letters*, 47(16), e2019GL086810. <https://doi.org/10.1029/2019gl086810>
- Andrews, J., & Barry, R. (1978). Glacial inception and disintegration during the last glaciation. *Annual Review of Earth and Planetary Sciences*, 6(1), 205–228. <https://doi.org/10.1146/annurev.ea.06.050178.001225>
- Bahadory, T., Tarasov, L., & Andres, H. (2021). Last glacial inception trajectories for the Northern Hemisphere from coupled ice and climate modelling. *Climate of the Past*, 17(1), 397–418. <https://doi.org/10.5194/cp-17-397-2021>
- Balbon, E. (2000). Variabilité climatique et circulation thermohaline dans l’Océan Atlantique Nord et en Mer de Norvège au cours du Quaternaire Supérieur, Paris 11.
- Bartlein, P. J., & Shafer, S. L. (2019). Paleo calendar-effect adjustments in time-slice and transient climate-model simulations (PaleoCalAdjust v1.0): Impact and strategies for data analysis. *Geoscientific Model Development*, 12(9), 3889–3913. <https://doi.org/10.5194/gmd-12-3889-2019>
- Batchelor, C. L., Margold, M., Krapp, M., Murton, D. K., Dalton, A. S., Gibbard, P. L., et al. (2019). The configuration of Northern Hemisphere ice sheets through the Quaternary. *Nature Communications*, 10(1), 3713. <https://doi.org/10.1038/s41467-019-11601-2>
- Berger, A. (1978). Long-term variations of daily insolation and Quaternary climatic changes. *Journal of the Atmospheric Sciences*, 35(12), 2362–2367. [https://doi.org/10.1175/1520-0469\(1978\)035<2362:ltvodi>2.0.co;2](https://doi.org/10.1175/1520-0469(1978)035<2362:ltvodi>2.0.co;2)
- Born, A., Nisancioglu, K. H., & Braconnot, P. (2010). Sea ice induced changes in ocean circulation during the Eemian. *Climate Dynamics*, 35(7–8), 1361–1371. <https://doi.org/10.1007/s00382-009-0709-2>
- Calov, R., Ganopolski, A., Claussen, M., Petoukhov, V., & Greve, R. (2005). Transient simulation of the last glacial inception. Part I: Glacial inception as a bifurcation in the climate system. *Climate Dynamics*, 24(6), 545–561. <https://doi.org/10.1007/s00382-005-0007-6>
- Capron, E., Govin, A., Stone, E. J., Masson-Delmotte, V., Mulitza, S., Otto-Bliessner, B., et al. (2014). Temporal and spatial structure of multi-millennial temperature changes at high latitudes during the Last Interglacial. *Quaternary Science Reviews*, 103, 116–133. <https://doi.org/10.1016/j.quascirev.2014.08.018>
- Chen, G.-S., Kutzbach, J., Gallimore, R., & Liu, Z. (2011). Calendar effect on phase study in paleoclimate transient simulation with orbital forcing. *Climate Dynamics*, 37(9–10), 1949–1960. <https://doi.org/10.1007/s00382-010-0944-6>
- Clark, P., Clague, J., Curry, B. B., Dreimanis, A., Hicock, S., Miller, G., et al. (1993). Initiation and development of the Laurentide and Cordilleran ice sheets following the last interglaciation. *Quaternary Science Reviews*, 12(2), 79–114. [https://doi.org/10.1016/0277-3791\(93\)90011-a](https://doi.org/10.1016/0277-3791(93)90011-a)
- Cortijo, E., Lehman, S., Keigwin, L., Chapman, M., Paillard, D., & Labeyrie, L. (1999). Changes in meridional temperature and salinity gradients in the North Atlantic Ocean (30–72 N) during the last interglacial period. *Paleoceanography*, 14(1), 23–33. <https://doi.org/10.1029/1998pa090004>
- Danilov, S., Sidorenko, D., Wang, Q., & Jung, T. (2017). The finite-volume sea ice–ocean model (fesom2). *Geoscientific Model Development*, 10(2), 765–789. <https://doi.org/10.5194/gmd-10-765-2017>
- De Noblet, N. I., Prentice, I. C., Joussaume, S., Texier, D., Botta, A., & Haxeltine, A. (1996). Possible role of atmosphere-biosphere interactions in triggering the Last Glaciation. *Geophysical Research Letters*, 23(22), 3191–3194. <https://doi.org/10.1029/96gl03004>
- Erb, M. P., Broccoli, A. J., & Clement, A. C. (2013). The contribution of radiative feedbacks to orbitally driven climate change. *Journal of Climate*, 26(16), 5897–5914. <https://doi.org/10.1175/jcli-d-12-00419.1>
- Gallimore, R., & Kutzbach, J. (1996). Role of orbitally induced changes in tundra area in the onset of glaciation. *Nature*, 381(6582), 503–505. <https://doi.org/10.1038/381503a0>
- Imbrie, J., Boyle, E., Clemens, S., Duffy, A., Howard, W., Kukla, G., et al. (1992). On the structure and origin of major glaciation cycles 1. Linear responses to Milankovitch forcing. *Paleoceanography*, 7(6), 701–738. <https://doi.org/10.1029/92pa02253>
- Irvahl, N., Ninnemann, U. S., Kleiven, H. K. F., Galaasen, E. V., Morley, A., & Rosenthal, Y. (2016). Evidence for regional cooling, frontal advances, and East Greenland Ice Sheet changes during the demise of the last interglacial. *Quaternary Science Reviews*, 150, 184–199. <https://doi.org/10.1016/j.quascirev.2016.08.029>
- Jackson, C., & Broccoli, A. (2003). Orbital forcing of Arctic climate: Mechanisms of climate response and implications for continental glaciation. *Climate Dynamics*, 21(7–8), 539–557. <https://doi.org/10.1007/s00382-003-0351-3>
- Jochum, M., Jahn, A., Peacock, S., Bailey, D. A., Fasullo, J. T., Kay, J., et al. (2012). True to Milankovitch: Glacial inception in the new community climate system model. *Journal of Climate*, 25(7), 2226–2239. <https://doi.org/10.1175/jcli-d-11-00044.1>
- Joussaume, S., & Braconnot, P. (1997). Sensitivity of paleoclimate simulation results to season definitions. *Journal of Geophysical Research: Atmospheres*, 102(D2), 1943–1956. <https://doi.org/10.1029/96jd01989>
- Kageyama, M., Charbit, S., Ritz, C., Khodri, M., & Ramstein, G. (2004). Quantifying ice-sheet feedbacks during the last glacial inception. *Geophysical Research Letters*, 31(24), L24203. <https://doi.org/10.1029/2004gl021339>
- Kageyama, M., Sime, L. C., Sicard, M., Guarino, M.-V., de Vernal, A., Schroeder, D., et al. (2020). A multi-model CMIP6 study of Arctic sea ice at 127 ka: Sea ice data compilation and model differences. *Climate of the Past Discussions*, 2020, 1–33.
- Köhler, P., Nehrass-Ahles, C., Schmitt, J., Stocker, T. F., & Fischer, H. (2017). A 156 kyr smoothed history of the atmospheric greenhouse gases CO₂, CH₄, and N₂O and their radiative forcing. *Earth System Science Data*, 9(1), 363–387. <https://doi.org/10.5194/essd-9-363-2017>
- Kremer, A., Stein, R., Fahl, K., Ji, Z., Yang, Z., Wiers, S., et al. (2018). Changes in sea ice cover and ice sheet extent at the Yermak Plateau during the last 160 ka—Reconstructions from biomarker records. *Quaternary Science Reviews*, 182, 93–108. <https://doi.org/10.1016/j.quascirev.2017.12.016>
- Kutzbach, J., & Gallimore, R. (1988). Sensitivity of a coupled atmosphere/mixed layer ocean model to changes in orbital forcing at 9000 years BP. *Journal of Geophysical Research*, 93(D1), 803–821. <https://doi.org/10.1029/jd093id01p00803>
- Lachniet, M., Asmerom, Y., Polyak, V., & Denniston, R. (2017). Arctic cryosphere and Milankovitch forcing of Great Basin paleoclimate. *Scientific Reports*, 7(1), 12955. <https://doi.org/10.1038/s41598-017-13279-2>
- Lambeck, K., Purcell, A., Funder, S., Kjaer, K. H., Larsen, E., & Møller, P. (2006). Constraints on the Late Saalian to early Middle Weichselian ice sheet of Eurasia from field data and rebound modelling. *Boreas*, 35(3), 539–575. <https://doi.org/10.1080/03009480600781875>
- Lohmann, G. (2017). Atmospheric bridge on orbital time scales. *Theoretical and Applied Climatology*, 128(3–4), 709–718. <https://doi.org/10.1007/s00704-015-1725-2>

- Mangerud, J., Dokken, T., Hebbeln, D., Heggen, B., Ingólfsson, Ó., Landvik, J. Y., et al. (1998). Fluctuations of the Svalbard–Barents Sea Ice sheet during the last 150 000 years. *Quaternary Science Reviews*, *17*(1–3), 11–42. [https://doi.org/10.1016/s0277-3791\(97\)00069-3](https://doi.org/10.1016/s0277-3791(97)00069-3)
- Mangerud, J., Jansen, E., & Landvik, J. Y. (1996). Late Cenozoic history of the Scandinavian and Barents Sea ice sheets. *Global and Planetary Change*, *12*(1–4), 11–26. [https://doi.org/10.1016/0921-8181\(95\)00009-7](https://doi.org/10.1016/0921-8181(95)00009-7)
- Mangerud, J., & Svendsen, J. I. (1992). The last interglacial-glacial period on Spitsbergen, Svalbard. *Quaternary Science Reviews*, *11*(6), 633–664. [https://doi.org/10.1016/0277-3791\(92\)90075-j](https://doi.org/10.1016/0277-3791(92)90075-j)
- Manthé, S. (1998). Variabilité de la circulation thermohaline glaciaire et interglaciaire en Atlantique Nord tracée par les foraminifères planctoniques et la microfaune benthique. Bordeaux 1.
- Meissner, K., Weaver, A., Matthews, H., & Cox, P. (2003). The role of land surface dynamics in glacial inception: A study with the UVic earth system model. *Climate Dynamics*, *21*(7–8), 515–537. <https://doi.org/10.1007/s00382-003-0352-2>
- Milankovitch, M. K. (1941). *Kanon der Erdbestrahlung und seine Anwendung auf das Eiszeitenproblem* (Vol. 133, pp. 1–633). Royal Serbian Academy Special Publication.
- Pollard, D., & Reusch, D. B. (2002). A calendar conversion method for monthly mean paleoclimate model output with orbital forcing. *Journal of Geophysical Research: Atmospheres*, *107*(D22), 4615. <https://doi.org/10.1029/2002jd002126>
- Sagoo, N., Storelvmo, T., Hahn, L., Tan, I., Danco, J., Raney, B., & Broccoli, A. J. (2021). Observationally constrained cloud phase unmasks orbitally driven climate feedbacks. *Geophysical Research Letters*, *48*(6), e2020GL091873. <https://doi.org/10.1029/2020gl091873>
- Shi, X., & Lohmann, G. (2016). Simulated response of the mid-Holocene Atlantic meridional overturning circulation in ECHAM6-FESOM/MPIOM. *Journal of Geophysical Research: Oceans*, *121*(8), 6444–6469. <https://doi.org/10.1002/2015jc011584>
- Shi, X., Lohmann, G., Sidorenko, D., & Yang, H. (2020). Early-Holocene simulations using different forcings and resolutions in AWI-ESM. *The Holocene*, *30*(7), 996–1015. <https://doi.org/10.1177/0959683620908634>
- Shi, X., Werner, M., Krug, C., Brierley, C. M., Zhao, A., Igbinsola, E., et al. (2022b). Calendar effects on surface air temperature and precipitation based on model-ensemble equilibrium and transient simulations from PMIP4 and PACMEDY. *Climate of the Past*, *18*(5), 1047–1070. <https://doi.org/10.5194/cp-18-1047-2022>
- Shi, X., Werner, M., Wang, Q., Yang, H., & Lohmann, G. (2022). Simulated mid-Holocene and last interglacial climate using two generations of AWI-ESM. *Journal of Climate*, *35*(23), 7811–7831. <https://doi.org/10.1175/jcli-d-22-0354.1>
- Sidorenko, D., Goessling, H. F., Koldunov, N., Scholz, P., Danilov, S., Barbi, D., et al. (2019). Evaluation of FESOM2.0 coupled to ECHAM6.3: Preindustrial and HighResMIP simulations. *Journal of Advances in Modeling Earth Systems*, *11*(11), 3794–3815. <https://doi.org/10.1029/2019ms001696>
- Stein, R., Fahl, K., Gierz, P., Niessen, F., & Lohmann, G. (2017). Arctic Ocean sea ice cover during the penultimate glacial and the last interglacial. *Nature Communications*, *8*(1), 373. <https://doi.org/10.1038/s41467-017-00552-1>
- Stevens, B., Giorgetta, M., Esch, M., Mauritsen, T., Crueger, T., Rast, S., et al. (2013). Atmospheric component of the MPI-M earth system model: ECHAM6. *Journal of Advances in Modeling Earth Systems*, *5*(2), 146–172. <https://doi.org/10.1002/jame.20015>
- Stokes, C. R., Tarasov, L., & Dyke, A. S. (2012). Dynamics of the North American ice sheet complex during its inception and build-up to the last glacial maximum. *Quaternary Science Reviews*, *50*, 86–104. <https://doi.org/10.1016/j.quascirev.2012.07.009>
- Svendsen, J. I., Alexanderson, H., Astakhov, V. I., Demidov, I., Dowdeswell, J. A., Funder, S., et al. (2004). Late Quaternary ice sheet history of northern Eurasia. *Quaternary Science Reviews*, *23*(11–13), 1229–1271. <https://doi.org/10.1016/j.quascirev.2003.12.008>
- Timm, O., Timmermann, A., Abe-Ouchi, A., Saito, F., & Segawa, T. (2008). On the definition of seasons in paleoclimate simulations with orbital forcing. *Paleoceanography*, *23*(2), PA2221. <https://doi.org/10.1029/2007pa001461>
- Valcke, S. (2013). The OASIS3 coupler: A European climate modelling community software. *Geoscientific Model Development*, *6*(2), 373–388. <https://doi.org/10.5194/gmd-6-373-2013>
- Van Nieuwenhove, N., Bauch, H. A., Eynaud, F., Kandiano, E., Cortijo, E., & Turon, J.-L. (2011). Evidence for delayed poleward expansion of North Atlantic surface waters during the last interglacial (MIS 5e). *Quaternary Science Reviews*, *30*(7–8), 934–946. <https://doi.org/10.1016/j.quascirev.2011.01.013>
- Vavrus, S. J. (1999). The response of the coupled arctic sea ice–atmosphere system to orbital forcing and ice motion at 6 kyr and 115 kyr BP. *Journal of Climate*, *12*(3), 873–896. [https://doi.org/10.1175/1520-0442\(1999\)012<0873:trotca>2.0.co;2](https://doi.org/10.1175/1520-0442(1999)012<0873:trotca>2.0.co;2)
- Xu, S., Krebs-Kanzow, U., & Lohmann, G. (2024). A seasonally delayed Sea Ice response and arctic amplification during the last glacial inception [Dataset]. *Zenodo*. <https://doi.org/10.5281/zenodo.10425116>
- Yoshimori, M., Reader, M., Weaver, A., & McFarlane, N. (2002). On the causes of glacial inception at 116 kaBP. *Climate Dynamics*, *18*(5), 383–402. <https://doi.org/10.1007/s00382-001-0186-8>
- Young, M., & Bradley, R. (1984). Insolation gradients and the paleoclimatic record. In *Milankovitch and climate: Understanding the response to astronomical forcing* (pp. 707–713). Dordrecht: Springer Netherlands.